Available online at www.sciencedirect.com
ScienceDirect
Polymer 49 (2008) 1685–1692
polymer
www.elsevier.com/locate/polymer

Branching and re-orientation of lamellar crystals in non-banded poly(butene-1) spherulites

Hiroshi Kajioka [a], Masamichi Hikosaka [b], Ken Taguchi [b], Akihiko Toda [b,*]

[a] Department of Physics, Graduate School of Science, Kyoto University, Kyoto 606-8502, Japan
[b] Graduate School of Integrated Arts and Sciences, Hiroshima University, 1-7-1 Kagamiyama, Higashi-Hiroshima 739-8521, Japan

Received 4 September 2007; received in revised form 21 January 2008; accepted 21 January 2008
Available online 3 February 2008

Abstract

The formation mechanism of non-banded polymer spherulites has been examined experimentally for isotactic poly(butene-1) grown from the melt by optical, atomic force, and transmission electron microscopies associated with quenching and chemical etching. At the growth front of the spherulites, the maximum width of lamellar crystals, λ_m, showed a square-root dependence on the growth rate. The dependence suggests an instability-driven branching. In terms of the correlation of lamellar orientation in the spherulites, an auto-correlation function has been determined from the image taken by polarizing optical microscopy. The correlation showed an exponential decay along the radial direction, and the correlation length was in proportion to λ_m. Those experimental evidences suggest that the structure is formed by the coupling of the branching instability and the random re-orientation of lamellar crystals on the occasion of branching in the non-banded spherulites of poly(butene-1).

Keywords: Spherulites; Fingering instability; Poly(butene-1)

1. Introduction

When crystallized from the melt, polymer crystals develop a higher-order structure of spherical aggregate called spherulite, which consists of chain folded lamellar crystallites [1–3]. The lamellar crystals undergo branching and non-crystallographic re-orientation to fill in the three-dimensional space of the spherulite. The mechanisms of branching and re-orientation of lamellar crystals are therefore the most essential factors for the formation of polymer spherulites, in general.

Concerned with the branching mechanism, Keith and Padden proposed the formation of fibrous texture consisting of the groups of lamellar crystals [4]. They postulated that the fibrous texture was formed by an instability at the growth front in the diffusion field of impurities interrupting crystallization. Experimentally, utilizing chemical etching [5], the lamellar morphology in spherulites has been examined by Bassett et al. [6–8]. They examined the width of individual lamellar crystals, based upon the expectation that the width corresponds to the characteristic length of the fibrous texture. The obtained dependence of the width on molecular weight or on crystallization temperature was, however, not strong enough for their interpretation of Keith and Padden's model. So far, there is no explanation for the branching mechanism confirmed by firm experimental evidences.

In terms of the re-orientation of lamellar crystals on branching, polymer spherulites can be classified into two types, those with and without concentric bands under polarizing optical microscopy (POM): banded spherulite and non-banded spherulite, respectively, as shown in Fig. 1. The characteristic feature of the banded spherulite is the periodic extinction pattern under POM, whereas that of non-banded spherulites is a patchy pattern of white and black areas thin and long in shape along the radial direction. It is supposed that the difference of the patterns stems from the manner of re-orientation of lamellar crystals on branching. In banded spherulites, the concentric pattern is developed due to the twisting correlation of lamellar crystallites along the radial direction [9–13], where

* Corresponding author. Tel.: +81 82 424 6558; fax: +81 82 424 0757.
E-mail address: atoda@hiroshima-u.ac.jp (A. Toda).

0032-3861/$ - see front matter © 2008 Elsevier Ltd. All rights reserved.
doi:10.1016/j.polymer.2008.01.066

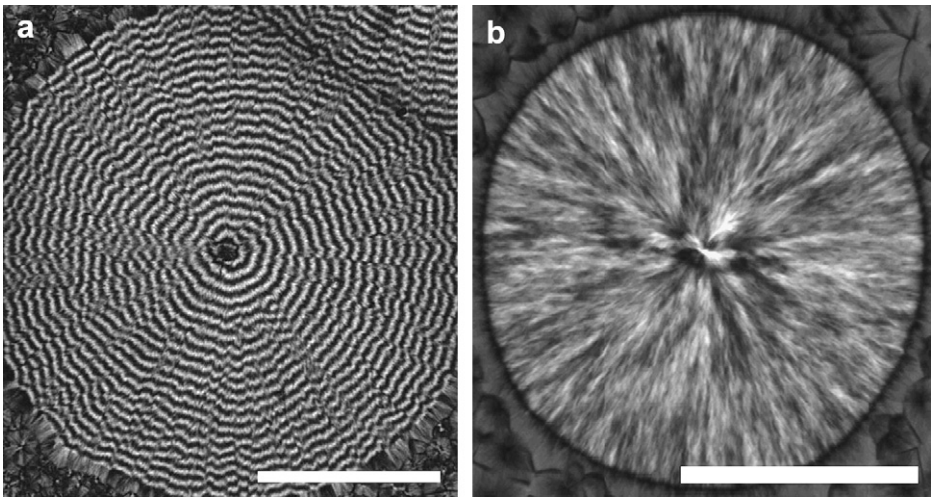

Fig. 1. Optical micrographs of (a) a banded spherulite of poly(vinylidene fluoride) and (b) a non-banded spherulite of poly(butene-1). The images were obtained by the sum of two images of the same area differing in the angle of polarizer by 45° while keeping the condition of cross-nicols. Scale bars represent 100 μm.

the correlation will hold on the occasion of branching. For non-banded spherulites, on the other hand, the direction of re-orientation must be randomly chosen on branching. Here, whereas the period of extinction bands can be easily measurable, the characteristic quantity of non-banded spherulites has not been well defined.

In the present paper, in order to understand the formation mechanism of the higher-order structure of polymer spherulites, the mechanisms of branching and re-orientation of lamellar crystals have been examined in non-banded spherulites. Firstly, we discuss the branching mechanism on the basis of the instability of growth front in a gradient field. The instability proposed by Keith and Padden will be reviewed in a wider class of fingering instability. Secondly, we define a persistence length of random orientation of lamellar crystals in non-banded spherulites. The persistence length characterizes the patchy pattern of non-banded spherulites such as shown in Fig. 1b. Experimentally, we examine the characteristic quantities such as the critical width of lamellar crystals at the growth front and the persistence length of lamellar orientation in the non-banded spherulites of isotactic poly(butene-1).

2. Modeling

2.1. Fingering instability

The most well-known instability of the growth front on crystallization is of Mullins and Sekerka's type in a diffusion field [14,15]. Generally, the diffusion field can be that of impurity or of temperature. The gradient of the diffusion field is characterized by a diffusion length, $\delta = D/V$, defined by the diffusion coefficient, D, divided by the growth rate, V. Due to slow growth rate of polymer spherulites, it is known that the thermal diffusion length is much larger than the size of ordinary spherulite, and hence the effect of temperature gradient is negligible on the morphological evolution of polymer spherulites. On the other hand, synthetic polymers inevitably have a molecular weight distribution and defects in chains, such as irregularity of tacticity, chemical branches, and tight entanglements. Actually, branched polyethylene shows the cellulation of spherulites due to the segregation of branches [16].

In the diffusion field with the compositional gradient at the growth front, the portions of the interface sticking out from neighboring area by fluctuations can grow faster because of the composition preferable for the crystallization. On the other hand, surface tension suppresses the growth of such protrusions. Then, the balance of those two effects determines the critical wavelength, λ_m, for the growth of the instability leading to branching. Based on the modeling of Mullins and Sekerka [14,15], the length, λ_m, depends on the mass diffusion length as,

$$\lambda_m \propto \left(\gamma \frac{D}{V}\right)^{1/2} \tag{1}$$

where γ represents the surface tension, V is the growth rate of the interface, and D is the mass diffusion coefficient. Such instability of growing interface in a gradient field is generally called fingering instability. For a lamellar crystal of finite width, the critical length, λ_m, corresponds to the maximum lateral width, beyond which the lamellar crystal undergoes branching.

The following questions may be raised in terms of the fingering instability of individual lamellar crystals. Firstly, for thin lamellar crystals, it seems that the formation of gradient field may not be probable if they are isolated in the bulk melt. However, at the growth front of spherulites, there are groups of lamellar crystals growing in parallel with each other. The gradient field can then be spontaneously formed and sustained by the stacks of those lamellar crystals. Each lamellar crystal feels the gradient of the field and undergoes the fingering instability on its own.

Secondly, polymer crystallization is known to be controlled by surface nucleation on the growth face [17] and not solely limited by diffusion. In this sense, the present argument on the morphological instability caused by the gradient field may be confusing. However, Goldenfeld [18] has theoretically suggested that the crystallization controlled both by the diffusion and by the surface kinetics can sustain stationary growth and undergo the morphological instability.

Our modeling for the formation of the higher-order structure of non-banded spherulites is based on the fingering instability, and is described as follows. On the occasion of branching, the crystals re-orient at a small angle and grow independently from each other in the three-dimensional space (Fig. 2). The non-crystallographic re-orientation is attributable to the strain caused by chain folding at the upper and lower surface regions of lamellar crystals [19] and to the pressure from uncrystallized molecular portions of cilia confined between lamellae [7]. The direction of re-orientation is chosen at random. Due to the independent growth of each lamellar crystal with re-orientation, the crystal can grow in width as well as in length. When the width reaches the critical width, the crystal undergoes the instability-driven branching again. In this way, the crystals sustain branching and re-orientation repeatedly. This mechanism will provide the branching frequency high enough to fill in the three-dimensional space of the spherulite with the non-crystallographic branching by the spontaneous re-orientation. In addition, a screw dislocation will be generated between neighboring branches as the consequence of the re-orientation on branching. The formation of screw dislocations therefore does not have to surmount the formation barrier with extremely large Burgers vector equal to the lamellar thickness [20].

2.2. Persistence length

In order to characterize the higher-order structure of non-banded spherulites, we examine auto-correlation functions of the intensity profile taken by POM. The auto-correlation function is defined as,

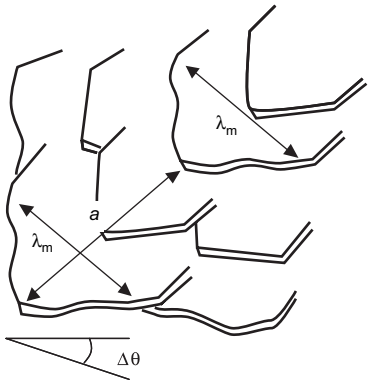

Fig. 2. Schematic illustration of lamellar branching with small angle re-orientation of the branches. Here, λ_m represents the critical width of fingering instability repeated at the distance, a, with the re-orientation angle, $\Delta\theta$.

$$C(d) = \frac{\langle I_x^{0.5} I_{x+d}^{0.5}\rangle - \langle I_x^{0.5}\rangle^2}{\langle I_x\rangle - \langle I_x^{0.5}\rangle^2} \tag{2}$$

where the angle brackets represent the statistical average, and I_x and I_{x+d} are the intensities at the positions x and $x+d$, respectively, displaced along the radial direction of a spherulite. The correlation function examines the characteristic feature of the patchy pattern seen in the non-banded spherulites along the radial direction (Fig. 1b).

For an optically uniaxial crystal, such as hexagonal (Form 1 [21]) and tetragonal (Form 2 [22]) crystal modifications of poly-(butene-1), the intensity taken by POM is expressed as [23],

$$I = I_0 \sin^2 2\mu \sin^2 \frac{\pi d(n_e - n_o)}{\lambda} \tag{3}$$

where I_0 represents the intensity of incident light, d is the sample thickness, n_o and n_e are the refractive indexes of ordinary and extraordinary rays, respectively, λ is the wavelength of incident light, and μ is the azimuthal angle between the axis of polarizer and the projection of the optical axis of the crystal onto the plane made by the axes of polarizer and analyzer. Eq. (3) indicates that the sum of the images, $I(\mu,\theta)+I(\mu+\pi/4,\theta)$, becomes independent of the azimuthal angle:

$$I' = I(\mu,\theta) + I(\mu+\pi/4,\theta) = I_0 \sin^2 \frac{\pi d(n_e - n_o)}{\lambda} \tag{4}$$

where the two images are of the same area differing in the angle of polarizer by 45° while keeping the condition of cross-nicols. The images of the banded and non-banded spherulites in Fig. 1 represent the results of this procedure. The Maltese cross disappears in the images being independent of the azimuthal angle of the crystals with respect to the polarizer. In the following, the correlation function of Eq. (2) is calculated for the intensity of the sum, I', obtained by this manner.

In Eq. (4), the refractive index of extraordinary ray, n_e, is given as [23],

$$n_e = \frac{n_o n_c}{\left(n_o^2 \sin^2\theta + n_c^2 \cos^2\theta\right)^{1/2}} \tag{5}$$

in terms of the refractive index along the optical axis of the crystal, n_c, that of ordinary ray, n_o, and the angle, θ, of the optical axis with respect to the propagation direction of light. Assuming small enough $x = \pi d(n_e - n_o)/\lambda$ and $n_c - n_o$, the square root of the intensity of Eq. (4) is approximated as,

$$I'^{0.5}(\theta) \cong I_0^{0.5} \frac{\pi d}{\lambda} |n_c - n_o| \sin^2\theta \tag{6}$$

The correlation function is then expressed as,

$$C(d) = \frac{\langle \sin^2\theta_x \sin^2(\theta_x+\delta_d)\rangle - \langle \sin^2\theta_x\rangle^2}{\langle \sin^4\theta_x\rangle - \langle \sin^2\theta_x\rangle^2} = \langle \cos 2\delta_d\rangle \tag{7}$$

under the assumption of no correlation between θ_x and δ_d. Here, θ_x is the angle at the position, x, and δ_d is the difference

of the angles at the distance, d, along the radial direction of a spherulite.

For a spherulite in a film much thinner than its radius, the angle of elevation or depression of the crystals is assumed to be negligible except for the central portion of the spherulite. The spherulite is then approximated as a two-dimensional spherulite, in which the angle, μ, corresponds to the azimuthal angle of growth direction of the crystal, and θ corresponds to the rotation angle of the crystal around the growth direction. The angle of rotation is supposed to undergo a discontinuous re-orientation on the occasion of branching. It is assumed that the direction of re-orientation is chosen at random around the radial axis with the interval, a, between branching, as shown in Fig. 2. The change in rotation angle is set at a small constant angle, $\Delta\theta$ (Fig. 2). For this type of re-orientation, by the analogy of random walk, the following relationship can be obtained,

$$\left\langle \delta_d^2 \right\rangle = N\Delta\theta^2, \quad N = \frac{d}{a} \tag{8}$$

where N is the number of the steps of branching. For $\langle\delta_d^2\rangle$ small enough, the auto-correlation function, $C(d)$, of Eq. (7) is approximated as,

$$C(d) \cong 1 - 2\left\langle \delta_d^2 \right\rangle \cong \exp\left[-\frac{d}{L}\right] \tag{9}$$

$$L \equiv \frac{a}{2\Delta\theta^2} \tag{10}$$

where L is defined as the persistence length of the rotation angle along the radial axis. This correlation length is similar to that obtained by light scattering [24], but is specified in the direction of the radial axis of a spherulite. It is noted that when fluctuations are introduced in $\Delta\theta$, the persistence length is inversely proportional to the mean square angle, $\langle\Delta\theta^2\rangle$.

The correlation function of Eq. (2) (and of Eq. (9)) is for one dimension along the radial axis of a spherulite. The following correlation function of the two-dimensional POM image of a spherulite well approximates the correlation function of Eq. (2), if the spherulite is large enough and the area is far from the center of the spherulite:

$$C(d) \cong \frac{1}{N_x N_y} \frac{\sum_x \sum_y \left(I'^{0.5}_{x,y} I^{0.5}_{x+d,y} - \left\langle I'^{0.5}_{x,y} \right\rangle^2 \right)}{\left\langle I'_{x,y} \right\rangle - \left\langle I'^{0.5}_{x,y} \right\rangle^2} \tag{11}$$

where N_x and N_y are the number of pixels in the image along the x ($\sim$radial direction of the spherulite) and y ($\sim$tangential) directions, respectively.

3. Experimental

3.1. Sample preparation

Isotactic poly(butene-1), PB-1, ($M_w = 674{,}000$, $M_w/M_n = 4.7$) was kindly supplied by Sun Allomer Ltd. With PB-1, it was easy to grow large spherulites ($\sim$1 mm) required for the assumption of two-dimensional spherulites and for the calculation of the auto-correlation function of the images. The films of 10–300 μm in thickness were prepared from the melt pressed between glasses or from *p*-xylene solution by solution casting. PB-1 films were melted at 160 °C and crystallized by a temperature jump to the crystallization temperature. The samples were then quenched into freezing acetone (−94 °C), if it was necessary to stop the growth. When PB-1 is crystallized from the melt, the metastable form, Form 2, is obtained [21,22] and then transforms to the stable form, Form 1 [25]. The crystallized samples were kept at room temperature more than a few days before examination in order to complete most of the transformation.

3.2. Width of lamellar crystals

For the examination of the width of flat-on lamellar crystals, PB-1 films of about 10 μm thick were crystallized. The films were then chemically etched to reveal the flat-on lamellar crystals on the free surface of the film: typical etchant consisted of 10 or 50 mg potassium permanganate, 6 ml orthophosphoric acid and 4 ml concentrated sulfuric acid [5]. The etched surface was observed with an atomic force microscope, AFM, (SPI3800 N, Seiko Instruments, Inc). Thick samples (200–300 μm) were also prepared and cut with an ultramicrotome (Ultra Cut, Leica) in order to examine the section of the lamellar crystals on the cut surface by transmission electron microscopy, TEM (JEOL100CX, JEOL Ltd.). As shown in Fig. 3, the length of the section parallel to the boundary of the spherulite corresponds to the width of the lamellar crystals on the cut surface.

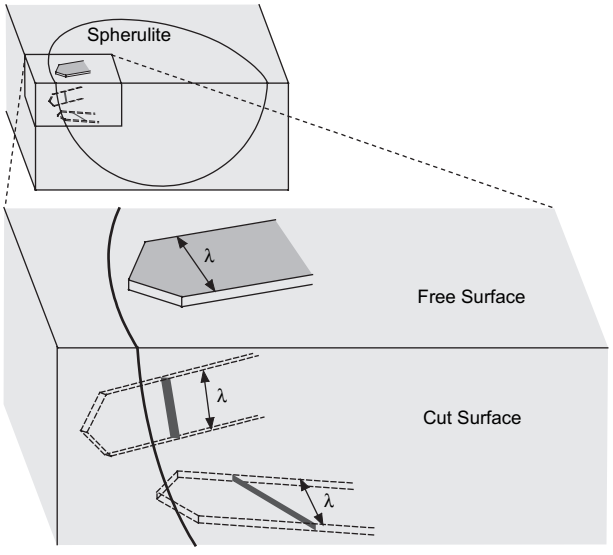

Fig. 3. Schematic illustration of lamellar crystals in a spherulite. The flat-on lamellar crystal on the top (free) surface corresponds to the images in Fig. 4 and the section of crystals on the side (cut) surface to the images in Fig. 5. Length of the section on the cut surface corresponds to the width of lamellar crystals, λ, when the line section is parallel to the boundary of the spherulite.

3.3. Persistence length

For the examination of the persistence length, films of 10 μm thick were prepared. The images were taken with a polarizing optical microscope, POM, (BX51, Olympus Co Ltd.) equipped with a monochromatic filter (IF550, Olympus Co Ltd.). The intensities, I and I', in Eqs. (2) and (11) therefore represent the brightness in the monochromatic mode. For the crystallized film of 10 μm thick, the optical retardation, $d(n_e - n_o)$, caused by the crystal birefringence was evaluated to be at most 100 nm from the change in the interference color with the insertion of a sensitive color plate. For the retardation, the value of $n_c - n_o$ will be much smaller than unity and the value of $x = \pi d(n_e - n_o)/\lambda$ is estimated to be less than 0.57 with $\lambda = 550$ nm. Then, the approximation of $\sin x \cong x$ employed in the derivation of Eq. (6) from Eq. (4) leads to the numerical error of at most 5%, which was acceptable for the calculation of the persistence length from the semi-logarithmic plots of the correlation function of $I'^{0.5}$ (Fig. 8).

For the calculation of the two-dimensional auto-correlation function, a rectangular area was chosen with the long axis in parallel with the radial direction of a spherulite and with the degree of arc from the center of spherulite within ±15°. This limitation was required for the one dimensional correlation function (Eq. (2)) approximated by the auto-correlation function of the image (Eq. (11)). The overall mean gradient of the intensity profile in the area was corrected by subtracting linear changes in both the x and y directions. While keeping the sample at room temperature after crystallization for a few days, the intensity of spherulites under POM became stronger, but the morphology did not change and the persistence length was kept unchanged.

4. Results and discussion

4.1. Width of lamellar crystals

Fig. 4 shows the AFM images of flat-on lamellar crystals at the growth front of spherulites. It is clearly seen that the width of the lamellar crystals becomes wider with increasing crystallization temperatures. The measurement of the width was sometimes not straightforward because of the stacking of lamellar crystals on each other. In order to overcome the difficulty, the cut surface of spherulites was also examined (Fig. 5). In Fig. 5, the dark thick lines represent the section of lamellar crystals. We measured the width of lamellar

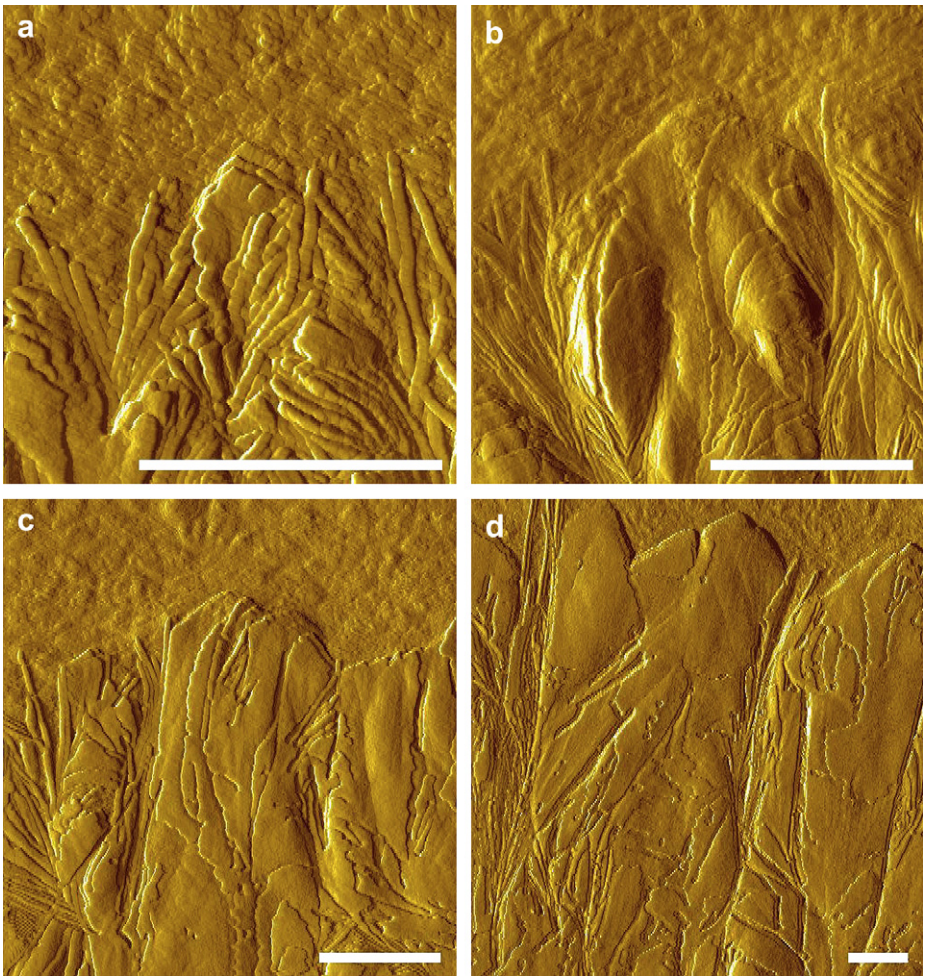

Fig. 4. AFM images (amplitude images) of the growth front of spherulites crystallized at (a) 86.5, (b) 91.5, (c) 96.5, and (d) 101.5 °C. Scale bars represent 2 μm.

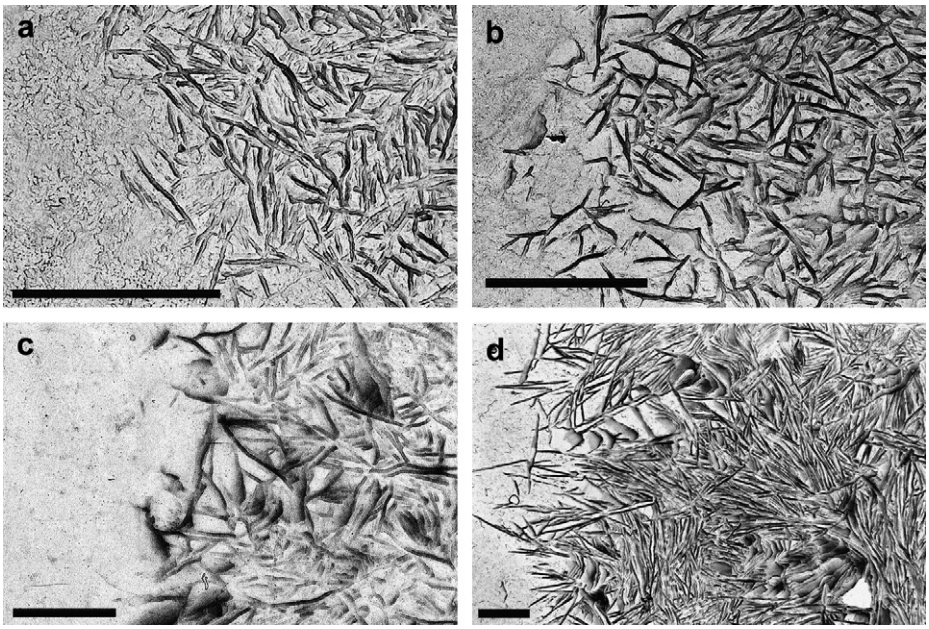

Fig. 5. TEM images of the replica of the cut surface of growth front of spherulites crystallized at (a) 86.5, (b) 91.5, (c) 96.5, and (d) 101.5 °C. Scale bars represent 2 μm.

crystals parallel to the rim of spherulites and chose the largest size from about 20 data at each crystallization temperature; the maximum width, λ_m, corresponds to the critical width of lamellar crystal just before branching due to instability, according to our model.

Fig. 6 shows the semi-logarithmic plots against $1/T\Delta T$ of the width, λ_m, and the growth rate, V, divided by the temperature dependence of the diffusion coefficient, D. Here, ΔT represents the degree of supercooling with the melting point of $T_m^0 = 130$ °C for the crystal Form 2 [26]. The WLF equation was utilized to estimate the temperature dependence of diffusion coefficient [17],

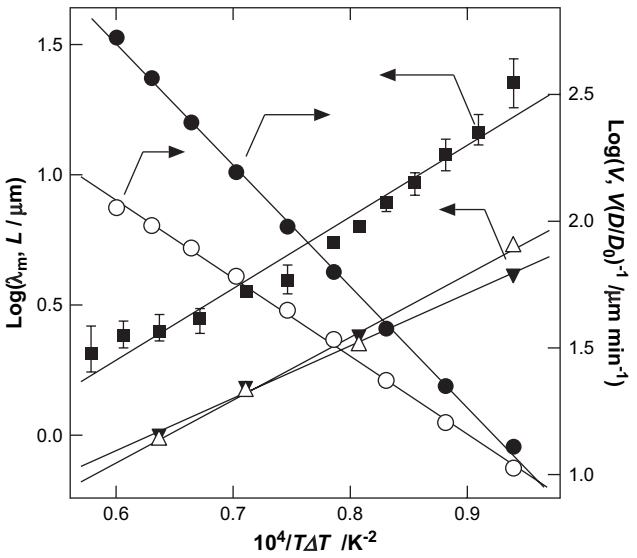

Fig. 6. Plots of λ_m determined from AFM (△) and TEM (▼), V (○) and $V(D/D_0)^{-1}$ (●), and L (■) against $1/T\Delta T$. The slopes of the fitted lines are 2.41 (λ_m from AFM), 2.01 (λ_m from TEM), −3.08 (V), −4.79 ($V(D/D_0)^{-1}$), and 2.75 (L). $V(D/D_0)^{-1}$ is divided by a constant, 10^5.

$$D = D_0 \exp\left[-\frac{U}{R(T - T_\infty)}\right] \tag{12}$$

with $U = 4120$ cal/mol, $T_\infty = T_g - 51.6$ °C, and the glass transition temperature, $T_g = -24$ °C [26].

The slopes of the fitted lines of the width, λ_m, and of the growth rate, $V(D/D_0)^{-1}$, in Fig. 6 were 2.41 (λ_m from AFM), 2.01 (λ_m from TEM), and −4.79 ($V(D/D_0)^{-1}$). The ratio between the slopes of λ_m and $V(D/D_0)^{-1}$ is close to 1:−2, as predicted from the fingering instability of Eq. (1) under the assumption of negligible changes in other factors, such as surface tension which actually has much weaker temperature dependence than V and D. To confirm the relation of Eq. (1), the measurement of the lamellar width at the growth front is essential; crystals in the inner part of spherulites can continue to grow in width after branching until the collision with other lamellae. It is also noted that the slope of the growth rate, V, in Fig. 6 is much smaller than that of $V(D/D_0)^{-1}$. The difference indicates the crucial contribution of D in the determination of the critical width of instability in Eq. (1).

In the present modeling of the fingering instability, our discussion is based on the instability of Mullins-Sekerka's type with the gradient of a compositional field. We may also think of another type of fingering instability similar to Saffman–Taylor instability [27] caused by a pressure gradient in a viscous fluid. For polymer crystallization, the pressure gradient is created in the melt in front of the growth face by the density difference between the crystalline and amorphous states [28]. The critical width, λ_m, is then in proportion to the inverse of the square root of the growth rate, V, and the viscosity of the fluid, η: $\lambda_m \propto [\gamma/(V\eta)]^{1/2}$. Due to the same temperature dependence of D and η^{-1} of WLF type, the instability by the pressure gradient predicts the same temperature dependence as that of the compositional gradient determined by Eqs. (1) and (12).

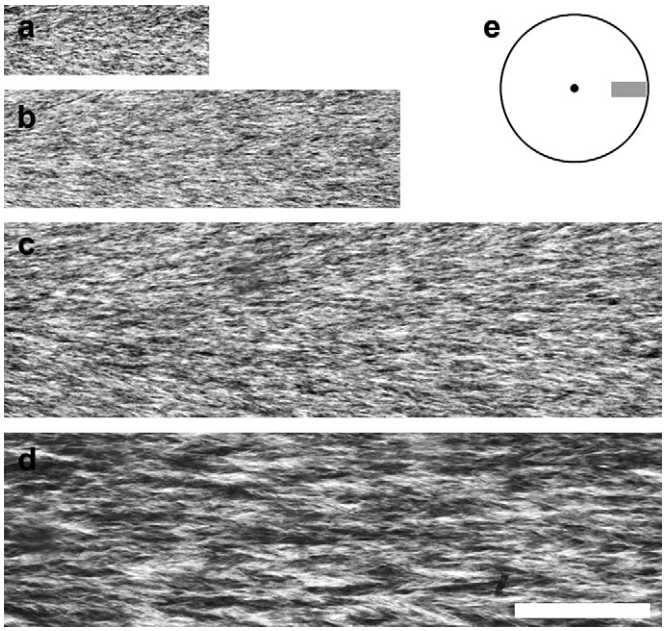

Fig. 7. POM images processed as described in text. Crystallization temperatures were (a) 86.5, (b) 91.5, (c) 96.5, and (d) 101.5 °C. The images are the portions of spherulites, as indicated in (e). Scale bar represents 100 μm.

4.2. Persistence length

Fig. 7 shows the POM images of the spherulites. It is clearly seen that the patchy texture becomes larger with increasing crystallization temperatures. Fig. 8 shows the profile of the auto-correlation function calculated from the POM images by using Eq. (11). The profile shows an exponential decay. The behavior suggests the random re-orientation of lamellar crystals along the radial direction in the non-banded spherulites of PB-1. The persistence length of Eq. (9) is determined from the slope in the semi-logarithmic plots of Fig. 8.

The persistence length represents the correlation of lamellar orientation along the radial direction of a spherulite. In the present modeling, the lamellar crystals are supposed to be re-oriented on the occasion of branching. Then, the persistence length can be interpreted in the following way on the basis of the fingering instability. Firstly, as shown in Fig. 2, the distance between successive branches, a, will be proportional to the critical width of lamellar crystals, λ_m, with a geometrical coefficient, g, determined by the axial ratio of growth rates,

$$a = g\lambda_m \tag{13}$$

Then, the persistent length, L, in Eq. (10) is proportional to λ_m, as follows,

$$L = \frac{g\lambda_m}{2\Delta\theta^2} \tag{14}$$

From Eqs. (1) and (14), under the assumption of much weaker dependencies of g and $\Delta\theta^2$ on the growth condition, such as crystallization temperature, than those of λ_m and D/V, we expect the proportional dependence of L on λ_m and the square-root dependence on D/V, as follows,

$$L \propto \lambda_m \propto \left(\frac{D}{V}\right)^{1/2} \tag{15}$$

Experimentally, Fig. 6 shows the plots of the persistent length, L, determined from the auto-correlation function in Fig. 8. By comparing the slope of L with those of λ_m and $V(D/D_0)^{-1}$ in Fig. 6, the ratio of the slopes of λ_m, $V(D/D_0)^{-1}$, and L is found to be close to 1:−2:1, as expected from Eq. (15). The dependence suggests the random re-orientation of lamellar crystals on the occasion of branching. Here, it is noted that, in a recent work of Gránásy et al. [29], they have suggested the crucial role of misorientation on branching for the formation of polymer spherulites at temperatures much higher than the glass transition temperature, $T_c > 1.2T_g$, while the misorientation was supposed to be caused by a grain nucleation near T_g [30]. The re-orientation of the present modeling can be the source of this type of misorientation on branching.

Based on the expression of Eq. (14), the absolute value of the branching angle, $\Delta\theta$, can be evaluated from the present experimental data, if the form factor, g, is available. The crystal Form 2 of PB-1 is tetragonal and the {100} growth facets are observed at the growth front, as shown in Fig. 4. If the branching occurs at the both sides of the growth face, as shown in Fig. 2, the form factor, g, in Eq. (14) becomes $g = 1/4$ and the following expression of $\Delta\theta$ is obtained from Eq. (14),

$$\Delta\theta = \frac{\lambda_m}{8L} \tag{16}$$

Fig. 9 shows the plots of the angle, $\Delta\theta$, determined from the experimental data of L and λ_m by using Eq. (16). The angle is in the range of 9–13° and keeps nearly constant value at lower crystallization temperatures and decreases at higher temperatures. Since the stress and pressure causing the re-orientation originate at the upper and lower surface regions of lamellar crystals, thicker lamellae are expected to be less susceptible to re-orientation on branching. Actually, the

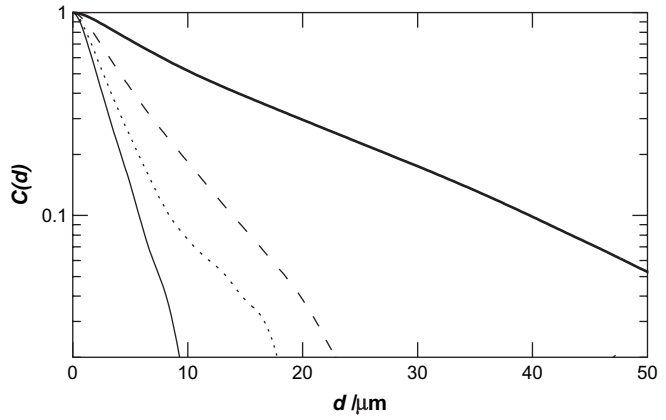

Fig. 8. Auto-correlation function, $C(d)$, determined from the images in Fig. 7 of PB-1 spherulites crystallized at (a) 86.5 (thin), (b) 91.5 (dotted), (c) 96.5 (broken), and (d) 101.5 °C (thick line). The functions were calculated for the areas longer than those shown in Fig. 7 by (a) 1, (b) 1.5, (c) 4, and (d) 7 times in the radial (horizontal) direction.

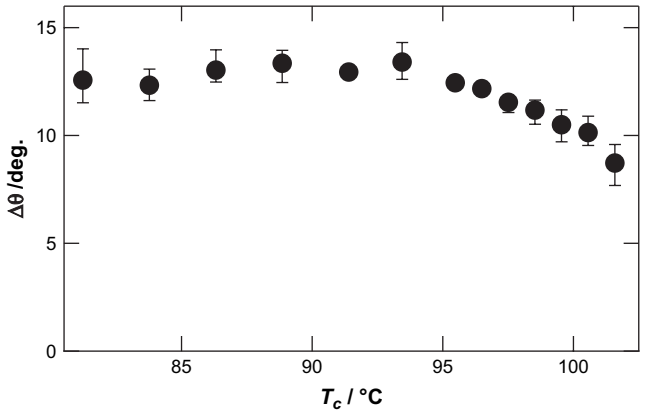

Fig. 9. Rotation angle, $\Delta\theta$, calculated by using Eq. (16) and plotted against crystallization temperature, T_c.

change in $\Delta\theta$ with temperature shown in Fig. 9 is in accordance with the change in lamellar thickness which is expected to increase at higher temperatures. The quantitative examination will need further theoretical formulation in terms of the determining mechanism of the angle $\Delta\theta$.

5. Conclusion

In terms of the branching and re-orientation of lamellar crystals in non-banded spherulites, the lamellar crystals and the spherulites of PB-1 have been examined experimentally. The maximum width of lamellar crystals at the growth front, λ_m, showed a square-root dependence on the growth rate. The dependence suggests the branching (fingering) instability caused by a gradient field ahead of the growth front. The possibilities of compositional gradient and pressure gradient have been discussed. The identification of the origin of the gradient field will be an important issue to be clarified in the future work.

For the higher-order structure of non-banded spherulites, the auto-correlation functions of POM images of spherulites have been examined. The correlation along the radial axis of spherulites showed an exponential decay. The behavior suggests a random re-orientation of lamellar crystals along the radial direction. The slope of the decay determines the persistence length, which characterizes the re-orientation and the consequent patchy pattern along the radial direction in non-banded spherulites. The persistence length of non-banded spherulites can therefore be considered as a counterpart of the period of extinction rings of banded spherulites. The persistence length of PB-1 spherulites was in proportion to λ_m. Based on the present modeling, the relationship suggests the random re-orientation on the occasion of branching.

For the formation of non-banded spherulites, the results suggest the essential role of the coupling between the fingering instability of growth front and the random re-orientation on the occasion of branching. For the banded spherulites of polyethylene [31] and poly(vinylidene fluoride) [32], our recent results confirmed the coupling between the fingering instability and the intrinsic torsional re-orientation expected for banded spherulites. Those are important evidences to understand the formation mechanism of polymer spherulites in general.

Acknowledgments

The authors are grateful to Dr. K. Yamada (Sun Allomer Ltd.) for the kind supply of poly(butene-1) and wish to thank Prof. S. Tanaka of Hiroshima University, Prof. Y. Yamazaki of Waseda University, and Prof. T. Taniguchi of Yamagata University for helpful discussions. This work was partially supported by MEXT Japan, Grant-in-Aid for Scientific Research on Priority Areas, ‘‘Creation of Non-equilibrium Soft Matter Physics’’.

References

[1] Geil PH. Polymer single crystals. New York: Wiley; 1963.
[2] Magill JH. J Mater Sci 2001;36:3143.
[3] Bassett DC. J Macromol Sci 2003;B42:227.
[4] Keith HD, Padden Jr FJ. J Appl Phys 1963;34:2409.
[5] Olley RH, Hodge AM, Bassett DC. J Polym Sci Polym Phys Ed 1979;17:627.
[6] Bassett DC, Hodge AM. Proc R Soc Lond Ser A 1981;377:61.
[7] Bassett DC, Olley RH. Polymer 1984;25:935.
[8] Bassett DC, Vaughan AS. Polymer 1985;26:717.
[9] Point JJ. Bull Acad R Bel 1953;41:982.
[10] Keith HD, Padden Jr FJ. J Polym Sci 1959;39:123.
[11] Price FP. J Polym Sci 1959;39:139.
[12] Keller A. J Polym Sci 1959;39:151.
[13] Fujiwara Y. J Appl Polym Sci 1960;4:10.
[14] Mullins WW, Sekerka RF. J Appl Phys 1963;34:323.
[15] Langer JS. Rev Mod Phys 1980;52:1.
[16] Abo el Maaty MI, Bassett DC, Olley RH, Jääskeläinen P. Macromolecules 1998;31:7800.
[17] Hoffman JD, Davis GT, Lauritzen Jr JI. Treatise on solid chemistry, vol. 3. New York: Plenum Press; 1976 [chapter 7].
[18] Goldenfeld N. J Cryst Growth 1987;84:601.
[19] Lotz B, Cheng SZD. Polymer 2005;46:577.
[20] Shultz JM, Kinloch DR. Polymer 1969;10:271.
[21] Natta G, Corradini P, Bassi IW. Nuovo Cimento Suppl 1960;15:52.
[22] Turner-Jones A. J Polym Sci Part B Polym Phys 1963;1:455.
[23] Born M, Wolf E. Principles of optics. Oxford: Pergamon; 1975 [chapter 14].
[24] Stein RS, Stidham SN. J Appl Phys 1964;35:42.
[25] Boor Jr J, Mitchell JC. J Polym Sci Part A Polym Chem 1963;1:59.
[26] Gaur U, Wunderlich B. J Phys Chem Ref Data 1983;12:29.
[27] Saffman PG, Taylor GI. Proc R Soc Ser A 1958;245:312.
[28] Schultz JM. Polymer crystallization. Oxford: Oxford University Press; 2001 [chapter 10].
[29] Gránásy L, Pusztai T, Tegze G, Warren JA, Douglas JF. Phys Rev E 2005;72:011605.
[30] Gránásy L, Pusztai T, Börzsönyi T, Warren JA, Douglas JF. Nature Mater 2004;3:645.
[31] Toda A, Okamura M, Taguchi K, Hikosaka M, Kajioka H. Macromolecules, in press.
[32] Toda A, Hikosaka M, Taguchi K, Kajioka H, submitted for publication.